



Full Text View

[Volume 30, Issue 7 \(July 2000\)](#)

Journal of Physical Oceanography

Article: pp. 1706–1721 | [Abstract](#) | [PDF \(654K\)](#)

Impact of Sea Level Assimilation on Salinity Variability in the Western Equatorial Pacific

Femke C. Vossepoel*

Delft Institute for Earth-Oriented Space Research, Delft, Netherlands, and Royal Netherlands Meteorological Institute, De Bilt, Netherlands

David W. Behringer

NOAA/National Centers for Environmental Prediction, Washington, D.C.

(Manuscript received March 9, 1999, in final form August 17, 1999)

DOI: 10.1175/1520-0485(2000)030<1706:IOSLAO>2.0.CO;2

ABSTRACT

In the primitive equation model for the tropical Pacific at the National Centers for Environmental Prediction, subsurface temperature observations are assimilated. The addition of TOPEX/Poseidon sea level observations to the NCEP assimilation scheme has resulted in large differences in sea level during 1996. These differences are suggested to be related to salinity variability.

A bivariate assimilation scheme is presented that corrects both temperature and salinity. The method is tested with synthetic data in an identical triplets experiment, in which a westerly wind burst is simulated. In this experiment, the correction of salinity improves the density simulation and attenuates errors in salinity. A four-year assimilation experiment with real data is performed to test the system's performance for 1993–96. In this experiment, the assimilation of TOPEX/Poseidon observations improves dynamic height simulation without degrading the temperature field. This application of altimetry improves the mean salinity in the western equatorial Pacific and leads to a more pronounced salinity variability in the ocean model.

1. Introduction

Assimilation of temperature observations in models of the tropical Pacific Ocean has led to improved simulation and forecasting of El Niño and the Southern Oscillation (ENSO) (e.g., [Chen et al. 1995](#); [Ji et al. 1998](#); [Kleeman et al. 1995](#);

Table of Contents:

- [Introduction](#)
- [The ocean analysis system](#)
- [Synthetic experiment](#)
- [Real data experiment](#)
- [Summary and discussion](#)
- [REFERENCES](#)
- [TABLES](#)
- [FIGURES](#)

Options:

- [Create Reference](#)
- [Email this Article](#)
- [Add to MyArchive](#)
- [Search AMS Glossary](#)

Search CrossRef for:

- [Articles Citing This Article](#)

Search Google Scholar for:

- [Femke C. Vossepoel](#)
- [David W. Behringer](#)

[Stockdale et al. 1998](#)). Subsurface temperature observations are readily available through the Tropical Ocean and Global Atmosphere–Tropical Ocean–Atmosphere (TOGA–TAO) program and Voluntary Observing Ships (VOS), and provide a good coverage of the equatorial Pacific (for an overview of the TOGA–TAO program see [McPhaden et al. 1998](#)). In addition to temperature observations, sea level observations from the TOPEX/Poseidon (T/P) altimeter are used to correct the temperature field in the tropical Pacific. This application of altimetric sea level improves analyses of the tropical Pacific ([Carton et al. 1996](#)), and has the potential to improve ENSO forecasting ([Fischer et al. 1997](#); [Ji et al. 2000](#)).

In a case study of the impact of sea level assimilation on ENSO forecasting at the National Centers for Environmental Prediction (NCEP), [Ji et al. \(2000\)](#) compared two assimilation runs. Both runs use in situ temperature data, but one also uses altimetric sea-level data while the other does not. In both assimilation runs, the observations were used to correct only the model temperature field. In the western equatorial Pacific, the comparison reveals an 8-cm difference in sea level for 1996 ([Ji et al. 2000](#)). This discrepancy appears to be related to the relatively fresh conditions in the western Pacific. In these experiments the introduction of T/P observations into the assimilation has improved the model sea level, but has degraded the model temperature field. Ji et al. conclude that this is the result of the assimilation system applying the wrong correction to temperature to compensate for an inaccurate representation of salinity in the model. This conclusion is supported by the work of [Maes \(1998\)](#) who showed that in 1996 the variability of salinity in the western equatorial Pacific can account for 5–10 cm of the variability in dynamic height. Both [Ji et al. \(2000\)](#) and [Maes \(1998\)](#) use conductivity–temperature–depth (CTD) observations to demonstrate the impact of salinity variability on sea level. The assimilation of T/P sea level observations places an integral constraint on the density, but not on the vertical structure of density. For example, the vertical density structure will be distorted if the temperature of the thermocline is altered to compensate for salinity variability in the surface layers. The result of the distortion will be errors in the zonal pressure gradient and the horizontal velocity field. To avoid such problems Ji et al. suggest the use of a bivariate scheme, that assimilates temperature and sea-level data and corrects both temperature and salinity. Others have also pointed out the importance of salinity correction in ocean data assimilation ([Cooper 1988](#); [Woodgate 1997](#)).

With the limited availability of salinity observations, indirect salinity estimation methods are being developed as an alternative approach to salinity estimation. While the method of [Vossepoel et al. \(1999\)](#) formulates a salinity correction on the basis of statistical assumptions, [Troccoli and Haines \(1999\)](#) use a more physical approach. The latter method assumes temperature–salinity (T – S) properties to be conserved, whereas the method of [Vossepoel et al. \(1999\)](#) assumes that variability in T – S correlations introduces salinity estimation errors. In the [Troccoli and Haines \(1999\)](#) method, which is a derivation of the [Cooper and Haines \(1996\)](#) assimilation scheme, the correction of temperature and salinity is equivalent to a vertical shift of the water column. The advantage of this approach is that it does not initiate convection in the model, which could generate new water masses. While [Vossepoel et al. \(1999\)](#) base the T – S correlation on climatology, [Troccoli and Haines \(1999\)](#) use CTD observations for this purpose. Assuming that T – S properties are conserved, their method can only account for T – S variability when experimental evidence is available ([Troccoli and Haines 1999](#)).

The [Cooper and Haines \(1996\)](#) assimilation method also forms the starting point for a salinity estimation technique developed by [Maes \(1999\)](#) who reconstructs temperature and salinity profiles with combined vertical modes of temperature and salinity. Using the same vertical modes, but a different estimation technique, [Maes et al. \(2000\)](#) performed a retrospective analysis of the salinity in the western tropical Pacific. Both [Maes \(1999\)](#) and [Maes et al. \(2000\)](#) base the salinity estimations on temperature observations only. Recently, the Maes et al. method has been adapted to include sea level height ([Maes and Behringer, 2000](#)). All indirect methods mentioned focus on the western equatorial Pacific as a test area because salinity variability in this region is large and relatively well observed. The western equatorial Pacific will also be the test area of the present paper, where the method of [Vossepoel et al. \(1999\)](#) will be tested as part of an assimilation scheme, both in a synthetic and a real case.

Salinity variability in the western equatorial Pacific is dominated by zonal displacements of the so called “fresh pool” ([Delcroix and Pincaut 1998](#); [Vialard and Delecluse 1998a,b](#)). This thin layer of relatively fresh water (below 35.0 psu) in the western equatorial Pacific seems to respond to wind changes by sliding on top of denser, saltier water below ([Lukas 1988](#); [Hénin et al. 1998](#)). Zonal displacements of the fresh pool at ENSO timescales are related to zonal advection, which results from the combined effect of equatorial jets and Kelvin and Rossby waves ([Delcroix and Picaut 1998](#)). These waves can be excited by westerly wind bursts (WWBs), which are strong anomalies of the normally easterly winds lasting typically one week (e.g., [Weller and Anderson 1996](#); [Harrison and Vecchi 1997](#)). An early study of the regional response of the western Pacific to a WWB has been documented by [McPhaden et al. \(1992\)](#). Other detailed investigations of the upper ocean structure in response to WWBs have been done in the framework of the TOGA Coupled Ocean–Atmosphere Response Experiment (COARE) program (e.g., [Wijesekera and Gregg 1996](#); [Weller and Anderson 1996](#); [Feng et al. 1998](#); [Huyer et al. 1997](#)). For a description of the COARE program, see [Webster and Lukas \(1992\)](#).

In the present paper, we simulate the oceanic response to a simplified WWB. This experiment is used to simulate salinity variability in the western Pacific fresh pool, making it possible to test the indirect salinity estimation method in an assimilation scheme. From the simulation run with WWB forcing, pseudo-observations of sea surface height and temperature are sampled and assimilated in two other runs with no WWB forcing. Monitoring the reconstruction of salinity variability in these two assimilation runs, we can evaluate the performance of the assimilation scheme. To test this performance in a more

realistic case, we carry out two assimilation runs for the period 1993–96. The overview of this paper is as follows: the ocean model and assimilation system are presented in [section 2](#), and the synthetic assimilation experiments are presented in [section 3](#). The real experiments are described in [section 4](#), followed by a summary and discussion in [section 5](#).

2. The ocean analysis system

NCEP’s ocean analysis system consists of two parts: an ocean general circulation model plus a three-dimensional variational assimilation system. The ocean model is derived from the Modular Ocean Model (version 1), developed at the Geophysical Fluid Dynamics Laboratory ([Bryan 1969](#); [Cox 1984](#); [Philander et al. 1987](#)) and adapted at NCEP for use in operational ENSO forecasting. The model is configured for the Pacific Ocean, from 120°E to 70°W, with a 1.5° zonal resolution. Latitudinal resolution in the region between 10°S and 10°N is $\frac{1}{3}^\circ$, gradually increasing to 1° poleward of 20° latitude. The model has 28 levels, 18 of them concentrated in the top 400 meters. The equation of state computes the density by fitting a third-order polynomial to the equation of state as formulated by UNESCO (see, e.g., [Gill 1982](#)). For a more detailed description of the model, see [Ji et al. \(1995\)](#). In the present study, an extra source term has been added to the prognostic salinity equation to relax the model salinity to estimates based on climatological T – S correlations from [Levitus and Boyer \(1994\)](#) and [Levitus et al. \(1994\)](#). The timescale for the T – S relaxation is 50 days. At the surface, the relaxation of salinity is combined with a salt flux forcing that consists of an evaporation minus precipitation estimate (for further specification of these fields, see the description of the experiments in [sections 3a](#) and [4a](#)).

The assimilation system is derived from the scheme by [Derber and Rosati \(1989\)](#) and adapted for use in the NCEP ocean analysis system ([Behringer et al. 1998](#)). The variational scheme uses a conjugent gradient method to minimize the following cost function ([Behringer et al. 1998](#)):

$$I = \frac{1}{2} \mathbf{T}^T \mathbf{E}_t^{-1} \mathbf{T} + \frac{1}{2} [\mathbf{D}(\mathbf{T}) - \mathbf{T}_o]^T \mathbf{F}^{-1} [\mathbf{D}(\mathbf{T}) - \mathbf{T}_o], \quad (1)$$

where the vector \mathbf{T} represents the correction to the first-guess model temperature field, and \mathbf{E}_t is the first-guess error covariance matrix. The vector \mathbf{T}_o denotes the difference between the temperature observations and the model first guess, \mathbf{D} is an interpolation operator from the model grid to the observation locations, and \mathbf{F} is the observation error covariance matrix for temperature. The matrices \mathbf{E}_t and \mathbf{F} determine the distribution and amplitude of the temperature correction, and normalize each term in [\(1\)](#). The definition of the matrix \mathbf{E}_t is an extension of the original formulation of [Derber and Rosati \(1989\)](#) so that the covariance between two points is given by

$$a(z) \exp \left[- \left(\frac{x^2}{b_x^2} + \frac{y^2}{b_y^2} \right) \cos^{-1} \phi \right], \quad (2)$$

where ϕ is the latitude. The parameters b_x and b_y are set so that the corrections will have a larger scale in the zonal direction than in the meridional direction. The function $a(z)$ is proportional to the square root of the local vertical temperature gradient. The observational errors are assumed to be uncorrelated so that the matrix \mathbf{F} is diagonal. Further details on the specification of these matrices can be found in [Behringer et al. \(1998\)](#).

To include a salinity correction in the assimilation scheme, the ocean analysis system described above is adjusted in two places. In the model, salinity is relaxed to climatological temperature–salinity correlations as described above ([Levitus and Boyer 1994](#); [Levitus et al. 1994](#)). In the assimilation, errors of the first-guess estimate are corrected by minimizing a new cost function.

As a first step, the T – S relaxation links subsurface salinity variability to variability in temperature at all depths below the surface. Although the T – S relaxation gives reasonably accurate salinity estimates, errors will still exist. These estimation errors will be reflected in the dynamic height difference between model and observations. This difference may also be affected by errors in the temperature field, although temperature is well sampled in the equatorial Pacific. As a consequence, we can use this difference to correct both the temperature and the salinity field by minimization of a new cost function. This cost function is formulated as follows:

$$+\frac{1}{2}[\mathbf{D}(\mathbf{x}) - \mathbf{x}_o]^T \mathbf{F}^{-1} [\mathbf{D}(\mathbf{x}) - \mathbf{x}_o], \quad (3)$$

where the vector \mathbf{x} is the correction to the first-guess model temperature and salinity field, \mathbf{E} is the first-guess error covariance matrix for temperature and salinity, and the vector $\delta\mathbf{Z}_o$ denotes the difference between the dynamic height deviations and the model first-guess dynamic height deviations. Dynamic height is determined to a reference depth of 500 meters. Further, \mathbf{D} is an interpolation operator from the model grid to the observation locations, \mathbf{L} is a linear operator which translates a vertical temperature and salinity correction into a dynamic height contribution, and \mathbf{G} is the observation error covariance matrix for dynamic height. The matrices \mathbf{E} , \mathbf{F} , and \mathbf{G} normalize each term in the cost function.

The cost function (3) looks very similar to (1), but includes an additional (observational) term ($\frac{1}{2}[\mathbf{D}(\mathbf{L}\mathbf{x}) - \delta\mathbf{Z}_o]^T \mathbf{G}^{-1} [\mathbf{D}(\mathbf{L}\mathbf{x}) - \delta\mathbf{Z}_o]$), that relates temperature and salinity corrections to dynamic height variations. The vector \mathbf{x}_o holds all available temperature and salinity observations. As salinity observations are not currently available on a near-real time basis, we will not take into account any salinity observations in this paper. As a consequence, the salinity correction is purely based on the altimeter observations.

The vertical error covariance matrix for the model temperature and salinity, \mathbf{E} , is based on the matrix \mathbf{E}_T in (1) plus an additional error covariance for salinity, \mathbf{E}_S . In the error covariance matrix, salinity corrections are assumed to be uncorrelated to temperature corrections. Here \mathbf{E}_S has a horizontal covariance structure identical to the temperature covariance as described in Eq. (2). Assuming that the first-guess salinity corresponds to a T - S estimate, the vertical covariance at each grid location is scaled by a vertical salinity error variance function that is derived from a statistical analysis of salinity estimation errors (Vossepoel et al. 1999). In this study, a 17-yr dataset of conductivity-temperature-depth observations was used to formulate vertical salinity correction profiles. The salinity estimation errors for the CTD profiles have been averaged in bins of 10° in longitude, and 2° latitude, and the resulting field has been decomposed in empirical orthogonal functions (EOFs). An example of the resulting EOF is given in Fig. 1. The first EOF in each bin explains between 60% and 80% of the variance of salinity estimation errors and has been used as a model for the vertical error variance, after interpolation to model grid locations. The profiles are characterized by a maximum amplitude in the mixed layer as is illustrated in Fig. 2. The shape and amplitude of the profiles vary with geographical location and reflect the dominant physical processes. For example, the maximum at thermocline depth that is evident in particular profiles reflect variability in the T - S relation that occurs as a result of advection of the subsurface salinity maximum (e.g., Donguy et al. 1986), while a large amplitude at the surface may reflect T - S variability related to precipitation. Since there were not enough profiles available outside of 10° latitude, the salinity assimilation is restricted to the equatorial band (10°S - 10°N). For details on these correction profiles, see (Vossepoel et al. 1999).

The observational errors of the altimeter are assumed to be uncorrelated, hence \mathbf{G} is a diagonal matrix. The matrices \mathbf{F} and \mathbf{G} are modified to weigh data within a specified time window. In this paper, the time window is two weeks for all data. Data further away in time will have lower weights. The manner in which the matrices are adapted for this temporal weighting is described in Derber and Rosati (1989).

3. Synthetic experiment

a. Description of the experiment

The assimilation system is tested with a synthetic experiment in the western equatorial Pacific. The objective of the experiment is to evaluate the salinity correction in the bivariate scheme as compared to the univariate scheme in a situation where the truth is known. Therefore, a model truth run was designed to produce a strong variability in salinity. The output of the truth run was sampled and these data were assimilated in two other runs, one univariate and one bivariate. These three runs together form a triplets experiment. By comparing the model state of both assimilation runs with the truth run, it is possible to investigate the performance of the assimilations with regard to salinity estimation. In addition to the triplet runs a reference run, forced with climatological fields was also made. A schematic of the synthetic experiment is given in Fig. 3 and an overview of the model runs is provided in Table 1.

The set of initial conditions for all of the runs was obtained by spinning up the ocean with climatological forcing for five years. The forcing fields consist of climatological wind stress from Hellerman and Rosenstein (1983), climatological heat fluxes and shortwave radiation from Oberhuber (1988) and a climatological salt flux. The salt flux is composed of a climatological average of the 1979-95 composite precipitation data, known as the Climate Prediction Center Merged Analysis of Precipitation of Xie and Arkin (1997), combined with an average for the same period of the evaporation fields from the atmospheric reanalysis of NCEP (Kalnay et al. 1996). The reference run, or ‘‘Synthetic Control Run’’ (SCR), is an extension of the spinup using the same forcing fields.

The truth run, or “Synthetic wind stress Anomaly Run” (SAR), is similar to SCR, differing only in the wind stress forcing. The anomalous wind stress in SAR results from an idealized westerly wind burst derived from a description by [Harrison and Vecchi \(1997\)](#), hereafter HV). The description is based on a data analysis and is given by the equation

$$U(x, y, t_n) = U_0 \exp\left[-\left(\frac{x - X_0 + c_x t}{L_x}\right)^2\right] \times \exp\left[-\left(\frac{y - Y_0 + c_y t}{L_y}\right)^2\right] \exp\left[-\left(\frac{t_n}{T}\right)\right], \quad (4)$$

where U is the model zonal wind anomaly field, U_0 is the maximum anomaly at the point (X_0, Y_0) , (c_x, c_y) is the translational velocity, (L_x, L_y) are the spatial e -folding scales, T is the temporal e -folding scale, and $x, y,$ and t_n are the zonal location, meridional location and day, respectively. Following model “C” (Table 3 of HV), X_0 was set to 170°E, Y_0 to 0°, c_x and c_y to 0.0. The spatial scale L_x is 1.8×10^6 m, and L_y is 0.6×10^6 m. As an average value for U_0 , HV give 6.4 m s^{-1} , while the time scale T in HV is set to 3 days.

To simulate a strong WWB event, we chose a U_0 value of 10 m s^{-1} , and a timescale T of 10 days. To compute wind stress from this value for U_0 we used an empirical relationship given by $\tau = C_D \rho U_0^2$ (e.g., [Gill 1982](#)), where τ is the wind stress, ρ is the density of air, and C_D the drag coefficient. Choosing a value for C_D of 1.44×10^{-3} and a value for ρ of 1.25 kg m^{-3} , we found a corresponding wind stress of 0.18 N m^{-2} . The amplitude and timescale of our WWB model are not uncommon ([Keen 1987](#); [Harrison and Vecchi 1997](#); [Hartn 1996](#)). For example, in early January 1993 a wind burst was observed with a maximum point anomaly of 14.8 m s^{-1} , and duration of 11.5 days (HV). The zonal wind stress anomaly applied in SAR is given in [Fig. 4](#).

The model output of SAR is sampled and used as pseudo-observations in the assimilation runs. The temperature and dynamic height pseudo-observations are determined from weekly averaged SAR model fields in the region between 10°S and 10°N. Surface observations of temperature (SST) and dynamic height (DH) are sampled at one degree intervals. The temperature profiles are sampled at intervals of two degrees in meridional and nine degrees in zonal directions. To avoid singularities in the observational error covariance matrices, a 0.1°C error is assumed for temperature observations and a 0.5-cm error for dynamic height observations. This corresponds to roughly 5% of the total variability of temperature and dynamic height respectively.

The two assimilation runs which complete the set of triplets were forced with the same climatological fields as the reference run, SCR. In the Synthetic Temperature assimilation run (ST) only temperature observations were assimilated and the cost function (1) was used. In the Synthetic Temperature and Dynamic height assimilation run (STD) both temperature and dynamic height observations were assimilated and the cost function (3) was used.

b. Results

The ability of the assimilation runs, ST and STD, to reproduce the ocean state in the truth run, SAR, is evaluated by comparing the anomalies of dynamic height, density, temperature, and salinity. SAR being a run with different forcing conditions than ST and STD, a perfect assimilation with errorless observations may not be able to exactly reconstruct the ocean state of SAR. We think that testing the ability of the assimilation scheme to reproduce the ocean response of SAR gives an impression of how the scheme may perform in a real case, where a large part of the errors in the simulation may be due to errors in wind stress forcing. Given that the assimilation scheme may not be able to reproduce the response to the different wind stress field, we can still interpret the difference between STD (or ST) and SAR as a measure of success of the assimilation. In this section, we will compare the anomalies in the truth run (SAR minus the reference SCR) with the anomalies in the assimilation runs (ST minus SCR and STD minus SCR).

In the dynamic height anomalies of SAR, the Kelvin wave response to the WWB is a positive dynamic height anomaly east of the date line, as is shown in [Fig. 5](#). The anomaly grows in amplitude to a maximum of 8.7 dyn cm in week 5 and travels eastward at a speed of roughly 3 m s^{-1} until it fades away in week 12 as a result of the diffusion and equatorial divergence in the model (not shown).

The assimilation runs are evaluated for the ocean state of week 5 when the dynamic height anomaly is at its maximum. [Figure 6](#) shows the anomalies in the truth run, SAR minus SCR. The anomaly in dynamic height ([Fig. 6a](#)) is reflected in a negative density anomaly ([Fig. 6b](#)), which is due to anomalous temperature and salinity ([Figs. 6c,d](#)). In the temperature response to the WWB, a downwelling Kelvin wave is evident. In the salinity response, a zonal displacement of the surface salinity front is apparent, as well as a corresponding fresh anomaly below the surface west of the front. This front denotes the border of the western Pacific fresh pool, and the effect of the WWB appears to be a zonal displacement of this pool.

When temperature observations from SAR are assimilated in ST ([Fig. 7](#)), the resulting dynamic height anomaly has features similar to those in the SAR anomaly. The suppression of the thermocline is clearly visible ([Fig. 7d](#)) and causes a considerable surface deformation ([Fig. 7a](#)), although the amplitude is less than in SAR (cf. [Fig. 6a](#)). The salinity anomaly, however, is not reproduced in ST. The temperature correction in ST will have a slight effect on salinity because of the T - S relaxation, but this is by no means enough to reconstruct the salinity anomaly at the surface. The errors in temperature ([Fig. 8d](#)) partly explain the errors in dynamic height in [Fig. 8a](#). Considering the density and salinity errors in [Figs. 8b and 8c](#), however, it is clear that part of the dynamic height error is related to discrepancies in the salinity field. The assimilation scheme clearly fails to reproduce the salinity variations in the truth run.

The reconstruction of the ocean state is improved in STD when dynamic height observations as well as temperature observations are included in the assimilation ([Fig. 9](#)). The use of dynamic height improves reconstruction of dynamic height anomalies, and the freshening of the upper ocean layers is clearly visible in both the salinity and the density plots ([Figs. 9b,c](#)). The temperature reconstruction is similar to ST, and the temperature anomaly is not greatly altered by the assimilation of dynamic height. Despite the salinity correction, salinity errors are still present in STD but are less than in ST, as can be concluded from [Fig. 10](#). The errors in dynamic height have been reduced from a maximum of 7 cm in ST to a maximum of 5 cm in STD. The reduction in dynamic height errors is associated with a reduction in density errors of 0.2 g m^{-3} . The salinity errors at the surface remain below 0.25 psu in run STD, while the salinity errors in ST have a maximum of 0.45 psu. The temperature errors for the two runs are of the same order of magnitude.

4. Real data experiment

a. Description of the experiment

To test the performance of the salinity correction in a realistic case, three assimilation runs were performed for the period 1993–96. The “Real Control Run” (RCR) starts from the same initial conditions as SCR, but is then forced with observed wind stress forcing ([Goldenberg and O’Brien 1981](#)), observed precipitation ([Xie and Arkin 1997](#)), evaporation from the reanalysis of [Kalnay et al. \(1996\)](#), climatological heat-fluxes ([Oberhuber 1988](#)), and relaxation to observed SST ([Reynolds and Smith 1994](#)). The “Real Temperature” assimilation run (RT) is forced with the same forcing fields as RCR except that, instead of relaxing the model to SST, the observed SST is used in the assimilation. In addition to SST, the subsurface observations of the TOGA–TAO array and the XBT observations of VOS are included in the assimilation. Only temperature is corrected in RT.


The “Real Temperature and Dynamic Height” assimilation run (RTD) is forced in the same way as RT, but T/P observations of sea surface height are assimilated as well as temperature observations and both temperature and salinity fields are corrected. In cost function (3), the T/P deviations from the mean are compared to model dynamic height deviations from the mean. These are determined from dynamic height estimates referred to a reference level of 500 m. In the Tropics variations in dynamic height referenced to 500 m agree very well with sea level variations observed by T/P ([Katz et al. 1995](#)). T/P deviations from the mean were determined relative to a 1993–95 mean. The scheme for the real experiment is given in [Fig. 11](#), and an overview of the real model runs is provided in [Table 2](#).



b. Results



The model results from RT and RTD for the period 1993–96 are compared with independent observations from the tide gauge network ([Wyrski 1979](#)) and CTDs compiled by ([Ando and McPhaden 1997](#)).

The tide gauge network makes it possible to evaluate the effect of sea level assimilation in RTD. [Figure 12](#) shows a model–data comparison of the deviations from mean sea level at four stations in the equatorial Pacific. Because salinity effects are largest in the western equatorial Pacific, we chose three stations in that region. For reference, a fourth station is chosen in the central Pacific. The stations are the same four that were used for model–data comparison by Ji et al. (2000): Kapingamarangi (1.1°N, 155°E), Nauru (0.5°S, 167°E), Tarawa (1.4°N, 173°E), and Kanton (2.8°S, 172°W). The results show that for the 1993–95 period, both RTD and RT agree with the observations within 3 to 5 cm. For 1996, the agreement for Kanton is still good, while the fit for the three western stations is significantly worse. This is in agreement with the

results of the comparison of tide gauges and assimilation runs in [Ji et al. \(2000\)](#).

Though differences between sea level for RTD and RT are small during 1993–95, there is a noticeable difference in 1996 at the three western stations ([Fig. 12](#) ). In this period, RTD sea level gives a closer fit to observations. This does not come as a surprise because T/P and tide gauge observations measure the same variable. At Kapingamarangi, RTD and the tide gauge deviations do not fit as well for 1996 as during 1993–95, and the salinity correction does not remove the complete 1996 sea level discrepancy. This may be related to salinity fluctuations at deeper depths, as will be discussed later. In contrast to these results, the addition of T/P data in the [Ji et al. \(2000\)](#) approach removes the discrepancy effectively by using T/P observations to correct the temperature field. However, the temperature analysis of Ji et al. was degraded by sea level assimilation, while this is not the case in RTD.

The differences in sea level between RTD and RT for these four stations are related to differences in model salinity. This is illustrated with the temperature and salinity evolution for Kapingamarangi and Nauru ([Figs. 13](#)  and [14](#) ). Temperature evolution for both model runs is very similar. The salinity variability of RTD however, is clearly more pronounced. We have attempted to test the reality of this salinity variability by comparing it to CTD data from [Ando and McPhaden \(1997\)](#), although this comparison is hampered by the sparse sampling of the CTDs.

We have used the observations of six cruises ([Ando and McPhaden 1997](#)) around the tide gauges stations at Nauru and Kapingamarangi providing a total of 30 CTD profiles within a distance of five degrees of the tide gauge stations. In [Figs. 15](#)  and [16](#)  we show six model–data comparisons, each representative for one of the observing periods. For the profiles around 155°E, which are close to Kapingamarangi, RTD clearly does better than RT in the upper layers of the model salinity field during March 1993 and April 1994. In both cases, RTD surface salinity is closer to observations than RT. The salinity variability between depth 200 and 250-m, however, is represented in neither of the two assimilation runs. Because the first-guess vertical error covariance has a maximum amplitude in the upper layers, the assimilation is unable to correct errors at larger depths.

The same problem occurs around 165°E. Clear examples are shown for April 1995 and July 1996. In both profiles, salinity differences between RTD and RT are only visible in the upper ocean layers, while in the CTD observations, salinity varies at deeper depths. A positive salinity anomaly at 200 m in July 1996 caused the RTD assimilation to overcorrect at the surface. A positive salinity anomaly at 200 m in April 1995 was compensated by a negative salinity anomaly near the surface. The corresponding dynamic height anomaly would be small, which may be the explanation for the undercorrection at the surface. In March 1993, the observed halocline lies much deeper than the modeled halocline. As a consequence, there will be a positive dynamic height difference between observed and modeled dynamic height. This difference resulted in a freshening of the surface salinity. The salinity correction is applied at the wrong depth and causes an underestimation of the surface salinity.

For April 1994 the corrected salinity profile in RTD is slightly worse than the uncorrected profile in RT. This may be related to the occurrence of salinity minima around depths 150 and 250-m. The simple vertical error covariance only includes the first mode of the salinity estimation error. Including more vertical EOFs in the vertical error covariance function may lead to a more complete representation. For example, [Maes \(1999\)](#) shows that at 165°E, six modes of his decomposition of the total salinity signal are required to explain the salinity variability.

The model–data comparison shows that the assimilation scheme used in RTD performs well when the salinity variability is confined to the surface layers. However, the comparisons also highlight two problems with the assimilation scheme. First, they show the need to improve the specification of the first-guess error covariance matrix. In RTD the assimilation scheme does a poor job correcting the salinity in the halocline when the halocline is below 100 m. The problem is that the specified error covariance has confined the salinity corrections too close to the surface. The apparent large variability of salinity in the model suggests that improving the error covariance specification will be a daunting task. The second problem is more fundamental and arises, for example, when salinity deviations in the halocline have the opposite sign from deviations in the mixed layer and their contributions to the dynamic height effectively cancel. In such instances there is no signal in the sea surface height that can be used to correct the model salinity field with our method. An alternative approach is suggested by [Maes \(1999\)](#). By combining vertical modes of temperature and salinity, his method is able to correct salinity through observations of temperature. Still, the problem of determining the vertical salinity structure will be heavily underdetermined. Therefore, we think the best solution to this problem is in situ observations of salinity.

5. Summary and discussion

a. Summary

A method has been developed to correct the salinity field with sea level observations in locations where temperature is well known. To project the dynamic height information onto the salinity field, a vertical correction function has been generated with a CTD analysis. This correction function is used as a vertical error covariance in the assimilation of dynamic height

observation.

The assimilation scheme is tested with an identical triplets experiment in which salinity variability has been generated by the simulation of a westerly wind burst. The dynamic height and temperature field of this experiment are sampled and assimilated in two assimilation runs. One of these assimilation runs uses temperature observations only and corrects only the temperature field (ST), while the other assimilates both temperature and dynamic height observations and corrects both the temperature and salinity fields (STD). Both assimilation runs simulate the temperature response to a westerly wind burst equally well. The addition of dynamic height observations in run STD results in a more complete representation of the salinity in the upper layers of the model. This gives a better representation of the density structure.

Similar results are found when the assimilation scheme is applied in a more realistic case. For the period 1993–96, two assimilation runs were performed. As in the synthetic runs, one run assimilates only temperature observations and corrects only the temperature field (RT), while the other assimilates both temperature and dynamic height observations and corrects both the temperature and salinity fields (RTD). Temperature analysis in both runs is almost identical. Sea level analysis for RTD is closer to independent tide gauge observations than RT. The difference in sea level is related to a difference in salinity variability. Comparison of the salinity field with independent CTD observations suggests that salinity simulation in the upper layers is improved with the addition of T/P observations. The salinity variability at depths below 100 m, however, cannot be corrected with the present error covariance structure.

b. Discussion

Improving the ocean's density structure by assimilation of sea level observations is not straightforward. Unlike temperature or salinity observations, which can be assimilated directly, the sea level information needs to be projected into the subsurface. Various techniques make use of a priori statistics to propagate the sea level signal to model layers below. (e.g., [Cooper and Haines 1996](#); [De Mey and Robinson 1987](#); [Rienecker and Adamec 1995](#)). Either by assimilating “synthetic profiles” or by formulating a vertical error covariance function, sea level differences are related to corrections in the subsurface density field of the ocean. In a number of tropical applications of altimetric data assimilation, sea level variations in the tropics are assumed to be dominated by variations in heat content ([Fischer et al. 1997](#); [Carton et al. 1996](#); [Ji et al. 2000](#)). To first order, this is a reasonable assumption. However, the assimilation of temperature alone may corrupt the model's physics, if the model salinity field is not updated simultaneously ([Cooper 1988](#); [Woodgate 1997](#)).

The density of the ocean is determined by both temperature and salinity, so sea level observations reflect changes in both fields. When salinity variations are neglected, and sea level observations are used as a proxy for heat content, temperature corrections based on sea level observations may be different than those based on (direct) temperature observations. If this is the case and temperature is corrected based on sea level, this may corrupt the temperature and, as a consequence, the density structure. For example, if density variations occur in the upper ocean as a result of zonal displacements of the fresh pool, corresponding variations in sea level could get translated in a temperature correction at thermocline depth and be interpreted as a vertical displacement of the thermocline. The compensation of the two components of density was also noted by [Maes \(1998\)](#), and may result in a simulation where surface density variations occur at the wrong depth. A more balanced approach would be to correct both temperature and salinity as we have done here.

Although in the present scheme the salinity is corrected, no observations of salinity are used. Such observations could be readily incorporated into the assimilation and might lead to better results. Recent efforts have been made to reconstruct sea surface salinity with the aid of precipitation fields and in situ observations ([Reynolds et al. 1998](#)) and to observe sea surface salinity by remote sensing techniques ([Le Vine et al. 1998](#)). In the preparatory phase of this study, we investigated the assimilation of sea level and temperature observations in a synthetic case where sea surface salinity (SSS) was known. The SSS information improved the analysis at the surface, but its contribution to the salinity estimation at lower levels remained relatively small. This result suggests that to fully correct salinity variability, subsurface observations are needed as well. Both in the synthetic and in the realistic experiment, it is shown that the present assimilation cannot capture the full complexity of the salinity signal. In particular, the salinity variability at thermocline depth or below is not reconstructed by our scheme. With no direct salinity observations used in the assimilation, the vertical structure of the salinity correction is determined by the error covariance matrix only. If we had a more complete set of subsurface data, we would be able to improve the vertical error covariance function and, if such data were available on a near-real time basis, like the temperature data from TOGA-TAO or the sea surface height data from TOPEX/Poseidon, we could include them in the assimilation and be able to correct the model salinity directly. However, as long as these observations are not available, we will have to find ways to infer salinity variability by other means.

Acknowledgments

The authors wish to thank Ming Ji, Dick Reynolds, Christophe Maes, and Ants Leetmaa for valuable discussions, and valuable suggestions for the manuscript. Part of this work has been done during visits from Femke Vossepoel to the Washington, D.C., area, partly made possible by Bob Cheney, who also provided the TOPEX/Poseidon data for this study.

CTDs were obtained from M. McPhaden and K. Ando. Femke Vossepoel thanks Laury Miller, Gerrit Burgers, and Peter Jan van Leeuwen for lively discussions and encouragement. The authors thank two anonymous reviewers for their helpful comments. Computing resources were provided by the Center for High Performance applied Computing (HPaC) of Delft University of Technology. Femke Vossepoel's Ph.D. project is funded by the Space Research Organization Netherlands, SRON EO-024.

REFERENCES

- Ando, K., and M. J. McPhaden, 1997: Variability of surface layer hydrography in the tropical Pacific ocean. *J. Geophys. Res.*, **102**, 23 063–23 078..
- Behringer, D. W., M. Ji, and A. Leetmaa, 1998: An improved coupled model for ENSO prediction and implications for ocean initialization. Part I: The ocean data assimilation system. *Mon. Wea. Rev.*, **126**, 1013–1021.. [Find this article online](#)
- Bryan, K., 1969: A numerical model for the study of the circulation of the world ocean. *J. Comput. Phys.*, **4**, 347–376..
- Carton, J., B. Giese, X. Cao, and L. Miller, 1996: Impact of TOPEX and thermistor data on retrospective analysis of the tropical Pacific Ocean. *J. Geophys. Res.*, **101**, 14 147–14 159..
- Chen, D., S. E. Zebiak, A. J. Busalacchi, and M. A. Cane, 1995: An improved procedure for El Niño forecasting: Implications for predictability. *Science*, **269**, 1699–1702..
- Cooper, M., and K. Haines, 1996: Altimetric assimilation with water property conservation. *J. Geophys. Res.*, **101** (C1), 1059–1077..
- Cooper, N. S., 1988: The effect of salinity in tropical ocean models. *J. Phys. Oceanogr.*, **18**, 697–707.. [Find this article online](#)
- Cox, M. D., 1984: A primitive, 3-dimensional model of the ocean. GFDL Ocean Group Tech. Rep. 1, 143 pp. [Available from Geophysical Fluid Dynamics Laboratory/NOAA, Princeton University, Princeton, NJ 08540.].
- Delcroix, T., and J. Picaut, 1998: Zonal displacement of the western equatorial Pacific “fresh pool.” *J. Geophys. Res.*, **103**, 1087–1098..
- De Mey, P., and A. Robinson, 1987: Assimilation of altimeter eddy fields in a limited-area quasi-geostrophic model. *J. Phys. Oceanogr.*, **17**, 2280–2293.. [Find this article online](#)
- Derber, J., and A. Rosati, 1989: A global oceanic data assimilation system. *J. Phys. Oceanogr.*, **19**, 1333–1347.. [Find this article online](#)
- Donguy, J.-R., G. Eldin, and K. Wyrki, 1986: Sea level and dynamic topography in the western Pacific during 1982–83 El Niño. *Trop. Ocean–Atmos. Newslett.*, **36**, 1–3..
- Feng, M., P. Hacker, and R. Lukas, 1998: Upper ocean heat and salt balances in response to a westerly wind burst in the western equatorial Pacific during TOGA COARE. *J. Geophys. Res.*, **103** (C5), 10 289–10 311..
- Fischer, M., M. Latif, M. Flügel, and M. Ji, 1997: The impact of data assimilation on ENSO simulations and predictions. *Mon. Wea. Rev.*, **125**, 819–829.. [Find this article online](#)
- Gill, A. E., 1982: *Atmosphere–Ocean Dynamics*. Academic Press, 662 pp..
- Goldenberg, S. B., and J. J. O’Brien, 1981: Time and space variability of the tropical Pacific wind stress. *Mon. Wea. Rev.*, **109**, 1190–1207.. [Find this article online](#)
- Harrison, D. E., and G. A. Vecchi, 1997: Westerly wind events in the tropical Pacific. *J. Climate*, **10**, 3131–3156.. [Find this article online](#)
- Hartten, L. M., 1996: Synoptic settings of westerly wind bursts. *J. Geophys. Res.*, **101** (D12), 16 997–17 019..
- Hellerman, S., and M. Rosenstein, 1983: Normal monthly wind-stresses over the world ocean with error estimates. *J. Phys. Oceanogr.*, **13**, 1093–1104.. [Find this article online](#)
- Hélin, Chr., Y. du Penhoat, and M. Ioualalen, 1998: Observations of sea surface salinity in the western Pacific fresh pool: Large-scale changes in 1992–1995. *J. Geophys. Res.*, **103** (C4), 7523–7536..
- Huyer, A., P. M. Kosro, R. Lukas, and P. Hacker, 1997: Upper ocean thermohaline fields near 2°S, 156°E during the Tropical Ocean and Global Atmosphere Coupled Ocean–Atmosphere Response Experiment, November 1992 to February 1993. *J. Geophys. Res.*, **102**, 12 749–12 784..

- Ji, M., A. Leetmaa, and J. Derber, 1995: An ocean analysis system for seasonal to interannual climate studies. *Mon. Wea. Rev.*, **123**, 460–481.. [Find this article online](#)
- , D. Behringer, and A. Leetmaa, 1998: An improved coupled model for ENSO prediction and implications for ocean initialization. Part II: The coupled model. *Mon. Wea. Rev.*, **126**, 1022–1034.. [Find this article online](#)
- , R. W. Reynolds, and D. Behringer, 2000: Use of TOPEX/Poseidon sea level data for ocean analysis and ENSO prediction: Some early results. *J. Climate*, **13**, 216–231.. [Find this article online](#)
- Kalnay, E., and Coauthors, 1996: The NCEP/NCAR 40-Year Reanalysis Project. *Bull. Amer. Meteor. Soc.*, **77**, 437–471.. [Find this article online](#)
- Katz, E. J., A. Busalacchi, M. Bushnell, F. Gonzalez, L. Gourdeau, M. McPhaden, and J. Picaut, 1995: A comparison of the ocean surface height by satellite altimeter, mooring, and inverted echo sounder. *J. Geophys. Res.*, **100**, 25 101–25 108..
- Keen, R. A., 1987: Equatorial westerlies and the Southern Oscillation. *Proceedings of the U.S. TOGA Western Pacific Air–Sea Interaction Workshop*..
- Kleeman, R., A. M. Moore, and N. R. Smith, 1995: Assimilation of subsurface thermal data into a simple ocean model for the initialization of an intermediate coupled ocean–atmosphere forecast model. *Mon. Wea. Rev.*, **123**, 3102–3113.. [Find this article online](#)
- Le Vine, D., M. Kao, R. Garvine, and T. Sanders, 1998: Remote sensing of ocean salinity: Results from the Delaware coastal current experiment. *J. Atmos. Oceanic Technol.*, **15**, 1478–1484..
- Levitus, S., and T. P. Boyer, 1994: *World Ocean Atlas 1994*, Vol. 4: *Temperature*, NOAA Atlas NESDIS 3, U.S Dept. of Commerce, Washington, DC, 117 pp..
- , R. Burgett, and T. P. Boyer, 1994: *World Ocean Atlas 1994*, Vol. 3: *Salinity*. NOAA Atlas NESDIS 3, U.S Dept. of Commerce, Washington, DC, 97 pp..
- Lukas, R., 1988: Freshwater input to the western equatorial Pacific ocean and air-sea interaction. *Proc. U.S. PRC Int. TOGA Symp.*, Beijing, China, China Ocean Press, 305–327..
- Maes, C., 1998: Estimating the influence of salinity on sea level anomaly in the ocean. *Geophys. Res. Lett.*, **25**, 3551–3554..
- , 1999: A note on the vertical scales of temperature and salinity and their signature in dynamic height in the western Pacific Ocean. Implications for data assimilation. *J. Geophys. Res.*, **104**, 11 037–11 048..
- , and D. Behringer, 2000: Using satellite-derived sea level and temperature profiles for determining the salinity variability: A new approach. *J. Geophys. Res.*, **105** (C4), 8537–8548..
- , — , R. W. Reynolds, and M. Ji, 2000: Retrospective analysis of the salinity variability in the western tropical Pacific Ocean using an indirect minimization approach. *J. Atmos. Oceanic Technol.*, **17**, 512–524..
- McPhaden, M. J., F. Bahr, Y. du Penhoat, E. Firing, S. P. Hayes, P. P. Niiler, P. L. Richardson, and J. M. Toole, 1992: The response of the western equatorial Pacific Ocean to westerly wind bursts during November 1989 to January 1999. *J. Geophys. Res.*, **97**, 14 289–14 303..
- , and Coauthors, 1998: The Tropical Ocean–Global Atmosphere observing system: A decade of progress. *J. Geophys. Res.*, **103** (C7), 14 169–14 240..
- Oberhuber, J. M., 1988: An atlas based on the “COADS” data set: The budgets of heat, buoyancy and turbulent kinetic energy at the surface of the global ocean. Max-Planck-Institut für Meteorologie Rep. 15, 20 pp. [Available from Max-Planck-Institut für Meteorologie, Bundesstrasse 55, 20146 Hamburg, Germany.]
- Philander, S. G. H., W. J. Hurlin, and A. D. Siegel, 1987: A model of the seasonal cycle in the tropical Pacific Ocean. *J. Phys. Oceanogr.*, **17**, 1986–2002.. [Find this article online](#)
- Reynolds, R. W., and T. M. Smith, 1994: Improved global sea surface temperature analysis using optimal interpolation. *J. Climate*, **7**, 929–948.. [Find this article online](#)
- , M. Ji, and A. Leetmaa, 1998: Use of salinity to improve ocean modelling. *Phys. Chem. Earth*, **23**, 545–555..
- Rienecker, M. M., and D. Adamec, 1995: Assimilation of altimeter data into a quasi geostrophic ocean model using optimal interpolation and EOFs. *J. Mar. Syst.*, **6**, 125–143..

Stockdale, T. N., D. L. T. Anderson, J. O. S. Alves, and M. A. Balmaseda, 1998: Global seasonal rainfall forecasts using a coupled ocean-atmosphere model. *Nature*, **392**, 370–373..

Troccoli, A., and K. Haines, 1999: Use of the temperature–salinity relation in a data assimilation context. *J. Atmos. Oceanic Technol.*, **16**, 2011–2025..

Vialard, J., and P. Delecluse, 1998a: An OGCM study for the TOGA decade. Part I: Role of salinity in the physics of the western Pacific fresh pool. *J. Phys. Oceanogr.*, **28**, 1071–1088.. [Find this article online](#)

—, and —, 1998b: An OGCM study for the TOGA decade. Part II: Barrier layer formation and variability. *J. Phys. Oceanogr.*, **28**, 1089–1106.. [Find this article online](#)

Vossepoul, F. C., R. W. Reynolds, and L. Miller, 1999: Use of sea level observations to estimate salinity variability in the tropical Pacific. *J. Atmos. Oceanic Technol.*, **16**, 1401–1415..

Webster, P. J., and R. Lukas, 1992: TOGA COARE: The Coupled Ocean–Atmosphere Response Experiment. *Bull. Amer. Meteor. Soc.*, **73**, 1378–1416.. [Find this article online](#)

Weller, R. A., and S. P. Anderson, 1996: Surface meteorology and air–sea fluxes in the western equatorial Pacific warm pool during the TOGA Coupled Ocean–Atmosphere Response Experiment. *J. Climate*, **9**, 1959–1990.. [Find this article online](#)

Wijesekera, H. W., and M. C. Gregg, 1996: Surface layer response to weak winds, westerly bursts, and rain squalls in the western Pacific warm pool. *J. Geophys. Res.*, **101** (C1), 1977–1997..

Woodgate, R. A., 1997: Can we assimilate temperature data alone into a full equation of state model? *Ocean Modelling* (unpublished manuscripts) **114**, 4–5..

Wyrtki, K., 1979: Sea level variations; monitoring the breath of the Pacific. *Eos, Trans. Amer. Geophys. Union*, **60**, 25–27..

Xie, P., and P. A. Arkin, 1997: Global precipitation: A 17-year monthly analysis based on gauge observations, satellite estimates and numerical model outputs. *Bull. Amer. Meteor. Soc.*, **78**, 2539–2558.. [Find this article online](#)

Tables

Table 1. Overview of the synthetic assimilation runs: *T* denotes temperature; DH, dynamic height data.

Run	Forcing	Assimilation
SCR	Clim. winds	None
SAR	Anom. winds	None
ST	Clim. winds	<i>T</i>
STD	Clim. winds	<i>T</i> and DH

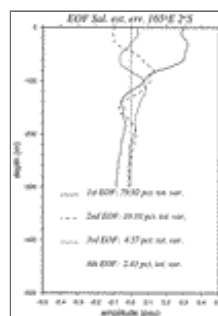
[Click on thumbnail for full-sized image.](#)

Table 2. Overview of the real assimilation runs: *T* denotes temperature; T/P, TOPEX/Poseidon sea level height observations.

Run	Forcing	Assimilation
RCR	Real winds	None
RT	Real winds	<i>T</i>
RTD	Real winds	<i>T</i> and T/P

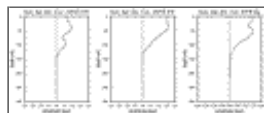
[Click on thumbnail for full-sized image.](#)

Figures



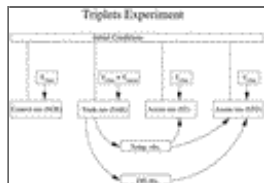
[Click on thumbnail for full-sized image.](#)

Fig. 1. The EOF decomposition for salinity estimation errors at 2°S, 165°E. The solid line denotes the first EOF, the dashed line the second EOF, and the gray line the third EOF. The percentage explained by the first four EOFs is given in the legend.



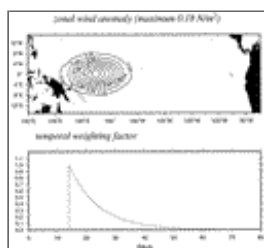
[Click on thumbnail for full-sized image.](#)

Fig. 2. Examples of the vertical error covariance function as a function of depth used for the salinity correction. Note that the horizontal axis is not the same for every figure panel.



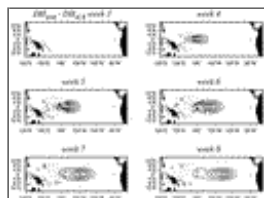
[Click on thumbnail for full-sized image.](#)

Fig. 3. Scheme for the triplets experiment: DH denotes dynamic height and τ denotes wind stress.



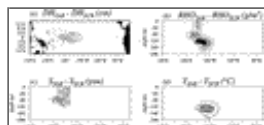
[Click on thumbnail for full-sized image.](#)

Fig. 4. Zonal wind stress anomaly imposed in truth run (SAR).



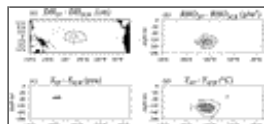
[Click on thumbnail for full-sized image.](#)

Fig. 5. Dynamic height response to the westerly wind burst for SAR (in cm).



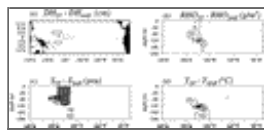
[Click on thumbnail for full-sized image.](#)

Fig. 6. Difference between the truth run and control run: (a) dynamic height, (b) density, (c) salinity, and (d) temperature along equator. A temperature difference of 1°C corresponds to a density difference of approximately 0.20 g m^{-3} . A salinity difference of 1 psu corresponds to a density difference of approximately 0.77 g m^{-3} .



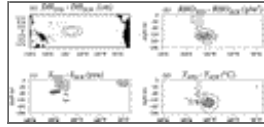
[Click on thumbnail for full-sized image.](#)

Fig. 7. Difference between ST and control run: (a) dynamic height, (b) density, (c) salinity, and (d) temperature along equator. A temperature difference of 1°C corresponds to a density difference of approximately 0.20 g m^{-3} . A salinity difference of 1 psu corresponds to a density difference of approximately 0.77 g m^{-3} .



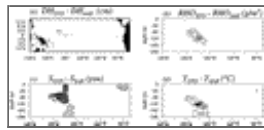
[Click on thumbnail for full-sized image.](#)

Fig. 8. Errors, or difference between ST and truth run: (a) dynamic height, (b) density, (c) salinity, and (d) temperature along equator. A temperature difference of 1°C corresponds to a density difference of approximately 0.20 g m⁻³. A salinity difference of 1 psu corresponds to a density difference of approximately 0.77 g m⁻³.



[Click on thumbnail for full-sized image.](#)

Fig. 9. Difference between STD and control run: (a) dynamic height, (b) density, (c) salinity, and (d) temperature along equator. A temperature difference of 1°C corresponds to a density difference of approximately 0.20 g m⁻³. A salinity difference of 1 psu corresponds to a density difference of approximately 0.77 g m⁻³.



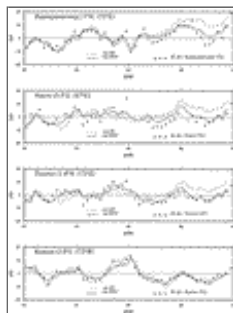
[Click on thumbnail for full-sized image.](#)

Fig. 10. Errors, or difference between STD and truth run: (a) dynamic height, (b) density, (c) salinity, and (d) temperature along equator. A temperature difference of 1°C corresponds to a density difference of approximately 0.20 g m⁻³. A salinity difference of 1 psu corresponds to a density difference of approximately 0.77 g m⁻³.



[Click on thumbnail for full-sized image.](#)

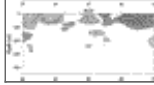
Fig. 11. Scheme for the real experiment: TP denotes TOPEX/Poseidon sea level observations.



[Click on thumbnail for full-sized image.](#)

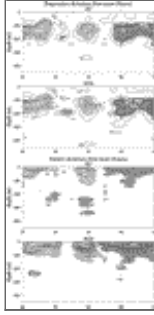
Fig. 12. Comparison of model runs vs tide gauges (TG) for RT: assimilation of temperature only and RTD: assimilation of temperature and T/P.





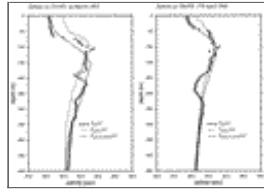
[Click on thumbnail for full-sized image.](#)

Fig. 13. Salinity and temperature deviations from mean at Kapingamarangi. Salinity values under -0.1 psu are shaded light gray, values over 0.1 dark gray. Temperature values under -1°C are shaded light gray, over 1°C dark gray.



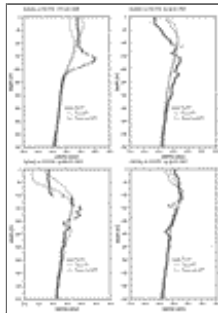
[Click on thumbnail for full-sized image.](#)

Fig. 14. Salinity and temperature deviations from mean at Nauru. Salinity values under -0.1 PSU are shaded light gray, values over 0.1 dark gray. Temperature values under -1°C are shaded light gray, over 1°C dark gray.



[Click on thumbnail for full-sized image.](#)

Fig. 15. Salinity profiles near Kapingamarangi. Crosses denote salinity observations from cruises in Mar 1993 and Apr 1994. The dashed line gives the monthly averaged salinity for RT; the gray line gives the monthly averaged salinity for RTD.



[Click on thumbnail for full-sized image.](#)

Fig. 16. Salinity profiles near Nauru for Jul 1996, Mar 1993, May 1995, and Apr 1994. Line types are similar as in [Fig. 15](#).

* Current affiliation: Laboratoire d'Océanographie Dynamique et de Climatologie/Université Pierre et Marie Curie, Paris, France.

Corresponding author address: Dr. Femke C. Vossepoel, Laboratoire d'Océanographie Dynamique et de Climatologie/Université Pierre et Marie Curie, Tour 26, 4eme Étage, 4 Place Jussieu, 75252 Paris Cedex 05, France. E-mail: femke.vossepoel@lodyc.jussieu.fr



DC Office: 1120 G Street, NW, Suite 800 Washington DC, 20005-3826
amsinfo@ametsoc.org Phone: 617-227-2425 Fax: 617-742-8718
[Allen Press, Inc.](#) assists in the online publication of *AMS* journals.